Ionization by Drift and Ambipolar Electric Fields in Electronegative Capacitive Radio Frequency Plasmas

J. Schulze,[1] A. Derzsi,[2] K. Dittmann,[3] T. Hemke,[4] J. Meichsner,[3] and Z. Donkó[2]

[1]*Institute for Plasma and Atomic Physics, Ruhr-University Bochum, Germany*
[2]*Research Institute for Solid State Physics and Optics, Hungarian Academy of Sciences, Hungary*
[3]*Institute of Physics, University of Greifswald, Germany*
[4]*Institute for Theoretical Electrical Engineering, Ruhr-University Bochum, Germany*

(Received 16 September 2011; published 28 December 2011)

Unlike α- and γ-mode operation, electrons accelerated by strong drift and ambipolar electric fields in the plasma bulk and at the sheath edges are found to dominate the ionization in strongly electronegative discharges. These fields are caused by a low bulk conductivity and local maxima of the electron density at the sheath edges, respectively. This drift-ambipolar mode is investigated by kinetic particle simulations, experimental phase-resolved optical emission spectroscopy, and an analytical model in CF_4. Mode transitions induced by voltage and pressure variations are studied.

DOI: 10.1103/PhysRevLett.107.275001 PACS numbers: 52.80.Pi, 52.27.Cm, 52.50.−b, 52.65.Rr

Charged particle kinetics in the space and time dependent electric fields of capacitively coupled radio frequency (CCRF) plasmas is a hot topic of current fundamental and applied research [1–4]. Such plasma sources are key elements for the production of various high technology products, e.g., solar cells, flat panel displays, and computer chips, since they allow etching and deposition processes on micro- to nanometer scales [5]. Miniaturized high pressure CCRF discharges, e.g., atmospheric pressure plasma jets (μ-APPJ), find medical and surface processing applications avoiding the necessity of expensive vacuum systems [6–8]. For these applications, the control of plasma properties, in particular, the particle flux-energy distributions at the substrate surface, is a central issue. Understanding the electron heating and ionization dynamics at the kinetic level is the basis for the optimization of plasma processes, since these dynamics determine the electron energy distribution function, which is crucial for the generation of excited species, ions, radicals, and the initiation of plasma chemical reactions.

There are two common operation modes of CCRF discharges [9]. (i) In the α mode, the ionization is dominated by electrons accelerated by the oscillating boundary sheath edges. This includes stochastic heating by the expanding sheaths [2] and electron heating due to field reversals during sheath collapse caused by electron inertia and/or electron-neutral collisions [4]. (ii) In the γ mode, the ionization is dominated by secondary electron avalanches inside the sheaths at times of high sheath voltage [9]. Transitions from the α to the γ mode are induced by increasing the voltage and/or pressure due to enhanced heating and multiplication of secondary electrons in the sheaths [9].

It is important to note that a high electron heating rate does not necessarily lead to a high ionization rate. Generally, the ionization depends on the dissipated power per electron rather than the total electron heating [10]. Thus, in low pressure electropositive discharges, Ohmic heating inside the bulk can be high, but does not cause significant ionization, since the deposited power is distributed to a high number of electrons. Typically, the bulk conductivity is high, the bulk electric field is low, and ionization due to electrons heated inside the bulk is not observed. Moreover, in electropositive plasmas, ambipolar fields accelerating electrons away from the adjacent electrode are observed at the sheath edges due to the strong local gradients of the electron density [4].

In electronegative and some molecular discharges, a high electric field, ionization rate, and average electron energy in the bulk have been observed [11–15]. It was demonstrated that this is a novel mode of discharge operation not related to the α and γ modes [14]. Moreover, local extrema of the electric field at the sheath edges accelerating electrons towards the adjacent electrode were observed [16]. However, the mechanisms causing these fields and, thus, the operation mode have not been clarified yet. Here, we study these mechanisms in CF_4 discharges with high electronegativity (between 10 and 45) by a combination of different approaches: (i) phase-resolved optical emission spectroscopy (PROES) measurements providing access to the spatiotemporal dynamics of highly energetic electrons within the rf period indicating the operation mode [3,17]; (ii) particle-in-cell (PIC) simulations, which provide a description of the plasma at the kinetic level and yield information about the spatiotemporal distribution of plasma parameters; and (iii) an analytical model to understand the formation of the electric field. This synergistic approach yields a coherent physical picture of a novel drift-ambipolar (DA) operation mode, which is expected to be valid also in electronegative discharges operated in gases other than CF_4.

We analyze the electron dynamics in CF_4 discharges with a gap of 1.5 cm, driven at 13.56 MHz, at different pressures and driving voltages. In the experiment, the plasma emission at 250 nm originating from dissociative deexcitation of excited CF_3^+ ions created by electron impact on CF_4 [18] is detected space resolved between the electrodes and time resolved within the rf period by PROES [3,17]. The plasma is confined between the electrodes by a fused silica cylinder to improve the discharge symmetry. The simulations are based on a 1D3V bounded electrostatic PIC code complemented with Monte Carlo treatment of collision processes. In order to compare the discharge behavior to that of electropositive gases, we carry out simulations of CF_4 and Ar discharges. In the case of CF_4, we trace CF_3^+, CF_3^-, F^- ions and electrons using cross sections and rate coefficients from [19]. For Ar, the cross sections are taken from [20]. The gas temperature is fixed at 350 K and the ion-induced secondary electron yield at the electrodes is $\gamma = 0.1$ in CF_4. Electrons hitting the electrodes are reflected with a probability of 20% and an ion-ion ($CF_3^+ + CF_3^-$, $CF_3^+ + F^-$) recombination rate of 5.5×10^{-13} $m^3\,s^{-1}$ is used [12].

Figure 1 shows simulation results for electropositive Ar and electronegative CF_4 discharges at 80 Pa. The first and second rows correspond to Ar discharges in the α mode ($\gamma = 0$, 100 V) and the γ mode ($\gamma = 0.2$, 200 V), respectively, while the third row shows results for a CF_4 discharge, where ionization inside the bulk and at the collapsing sheath edge is observed ($\gamma = 0.1$, 400 V, DA mode). The first column contains spatiotemporal plots of the electron heating rate, while columns 2–4 show the ionization rate, electric field, and electron density. In contrast to the electropositive discharges, the electron heating as well as ionization rate and the electric field are high inside the bulk in CF_4 at distinct times within one rf period. Similar to the electric field, the average electron energy is strongly modulated in the bulk between a minimum value of about 3 eV and a maximum value of about 7 eV at the time of strongest ionization. The electron density peaks at the sheath edges at times of small sheath width to ensure quasineutrality in the electropositive edge region of the discharge. The ionization rate increases towards the electrode, where the sheath is collapsing, and peaks close to the position of maximum electron density. The solid line in Fig. 2(a) shows the PIC result for the electric field at the time of strong ionization ($t \approx 26$ ns, marked by vertical black lines in Fig. 1) as a function of the distance from the powered electrode. The field is high and almost constant everywhere in the bulk except at the sheath edge close to the grounded electrode located at 1.5 cm, where its

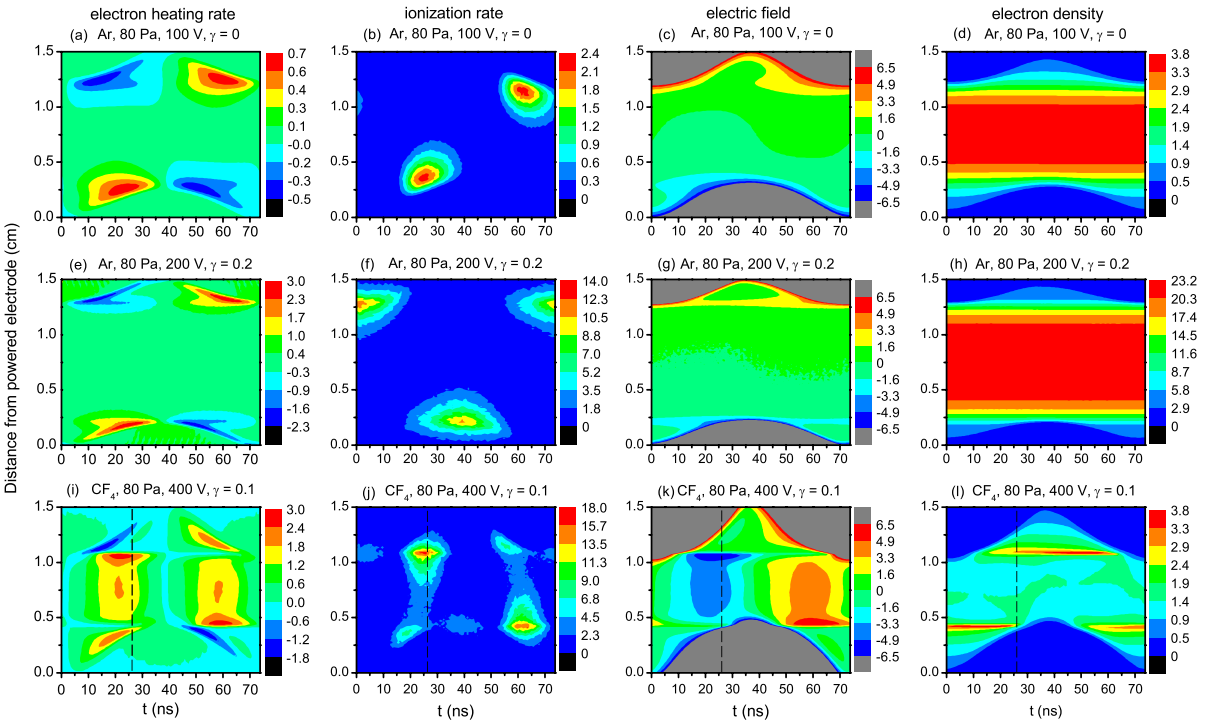

FIG. 1 (color online). PIC simulation results: spatiotemporal plots of the electron heating rate (first column), ionization rate (second column), electric field (third column), and electron density (fourth column) in Ar and CF_4 discharges driven at 13.56 MHz and 80 Pa with an electrode gap of 1.5 cm. First row: Ar, 100 V, $\gamma = 0$. Second row: Ar, 200 V, $\gamma = 0.2$. Third row: CF_4, 400 V, $\gamma = 0.1$. The color scales are given in units of 10^5 $W\,m^{-3}$ (heating rate), 10^{21} $m^{-3}\,s^{-1}$ (ionization rate), 10^3 $V\,m^{-1}$ (electric field), and 10^{15} m^{-3} (electron density).

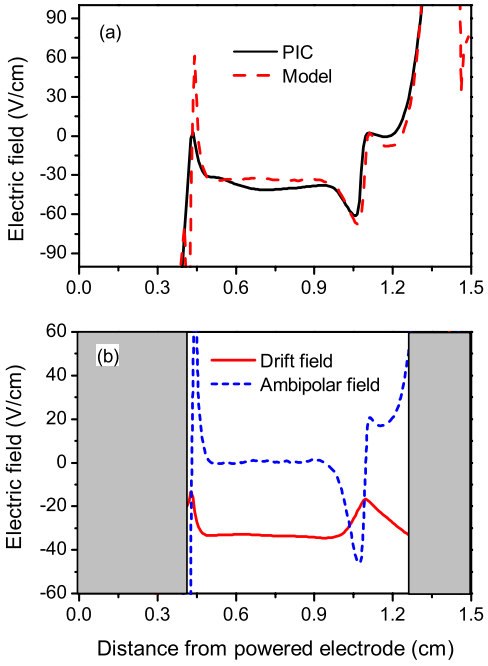

FIG. 2 (color online). Profiles of (a) the electric field obtained from the simulation (black solid line) and (1) (dashed red line); (b) the second (drift field) and fourth (ambipolar field) terms of (1) in the bulk at $t \approx 26$ ns [vertical dashed lines in Figs. 1(i)–1(l)]. Discharge conditions: CF_4, 13.56 MHz, 400 V, 80 Pa, $\gamma = 0.1$.

absolute value is maximum inside the bulk. The profile of the electric field resembles the profile of the ionization rate at this time.

In order to understand its physical origin, an analytical expression for the electric field is derived from the electron continuity and momentum balance equations [4]:

$$E = \frac{m_e}{n_e e^2}\left[\frac{\partial j}{\partial t} + \nu_c j + \frac{1}{e n_e^2}(j^2 - j_{\mathrm{th}}^2)\frac{\partial n_e}{\partial x} + \frac{jG}{n_e}\right], \quad (1)$$

with $j_{\mathrm{th}}^2 = \frac{e^2 n_e^2 k T_e}{m_e}$. Here m_e is the electron mass, e the elementary charge, n_e the electron number density, j the electron conduction current density, ν_c the electron-neutral collision frequency, G the ionization rate, and $kT_e = 2/3\langle\varepsilon_e\rangle$, where $\langle\varepsilon_e\rangle$ is the average electron energy. Applying this model at the time of strong ionization ($t \approx 26$ ns) and using input parameters from the simulation (n_e, j, ν_c, kT_e, G) yields the dashed line in Fig. 2(a), which is in very good agreement with the electric field resulting from the PIC simulation in the bulk region.

Discussing the individual terms of (1) [Fig. 2(b)] allows us to clarify the physical origin of the high electric fields in the bulk and at the sheath edges. Only the second (drift field) and fourth term (ambipolar field) of (1) are found to be important. All other terms are approximately zero and are not shown in Fig. 2(b). The second term yields the high and almost constant field in the discharge center, while the fourth term yields the local extremum of the field close to the sheath edge adjacent to the grounded electrode. Physically, the high bulk electric field is a drift field caused by a low dc conductivity $\sigma_{\mathrm{dc}} = \frac{n_e e^2}{m_e \nu_c}$. This high electric field accelerates electrons to high average energies and causes ionization in the bulk. σ_{dc} can be low due to (i) a low electron density, (ii) a high collision frequency, or (iii) a combination of both. In the electronegative CF_4 discharges discussed here, σ_{dc} is low in the bulk due to the low electron density [Fig. 1(l)]. The model predicts a high bulk electric field also for high values of ν_c, i.e., at high pressures, such as found in μ-APPJs. In fact, in these microdischarges, strong ionization and high electric fields in the bulk have been observed experimentally [7] and by simulations [8]. These results might also be explained qualitatively by our model.

The peak of the electric field at the sheath edge mainly results from the fourth term of (1), which corresponds to an ambipolar field. It is caused by a local maximum of the electron density at the sheath edge and the corresponding high value of $\partial n_e/\partial x$ [Fig. 1(l)] on the bulk side of this maximum. There, diffusion pushes the electrons into the bulk, while positive ions continuously flow towards the electrode. Thus, an ambipolar field is generated, that couples electron and positive ion motion and accelerates electrons towards the electrode. This is completely different to the situation in electropositive discharges, where the density gradient causes an ambipolar field, that accelerates electrons towards the discharge center. The electron heating and ionization at the collapsing sheath edge in the DA mode are highly transient phenomena, since a strong gradient of the electron density, a high average electron energy (ambipolar field), and a high discharge current (electron heating) are required in parallel.

Consequences of the drift and ambipolar electric fields predicted by the PIC simulation and understood by the analytical model are observed experimentally. Figure 3 shows the spatiotemporal ionization rate in CF_4 discharges operated at 40 Pa resulting from the PIC simulation (top row) and the spatiotemporal emission at 250 nm measured by PROES (bottom row) at different driving voltages. The DA mode is clearly observed experimentally at low voltages. By increasing the voltage, a transition from the DA- into the α mode is induced, since the sheath heating is enhanced. In the experiment, the discharge is asymmetric at high driving voltages due to the capacitive coupling between the dielectric confinement cylinder and the grounded chamber walls; i.e., a dc self-bias is generated. Therefore, there is no emission maximum at the top grounded electrode at 400 V.

Figure 4 shows the spatiotemporal ionization rate in CF_4 discharges operated at 200 V resulting from the PIC simulation (top row) and the measured emission (bottom row) at different neutral gas pressures. By increasing the pressure, a transition from a hybrid combination of the α and DA mode at low pressures into a pure DA mode is induced, since the electronegativity is increased as a

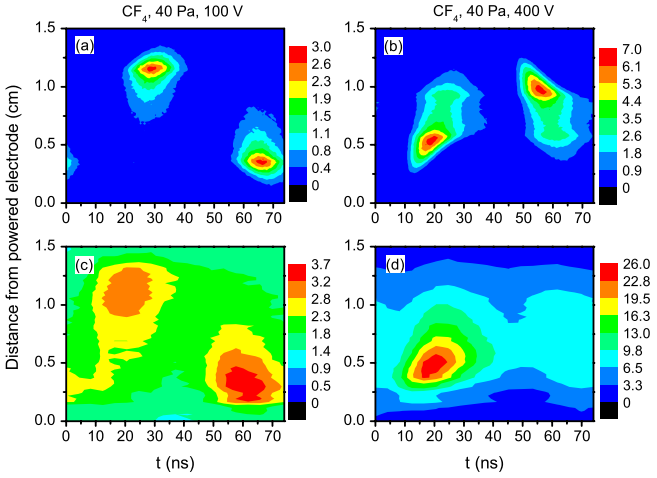

FIG. 3 (color online). Spatiotemporal ionization rate obtained from the simulation in units of 10^{21} m^{-3} s^{-1} (top row) and measured plasma emission at 250 nm in a.u. (bottom row) in a CF_4 discharge at different voltage amplitudes (13.56 MHz, 40 Pa).

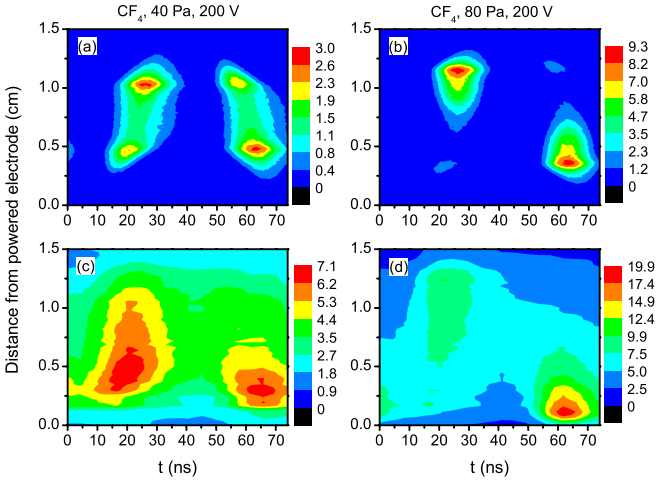

FIG. 4 (color online). Spatiotemporal ionization rate obtained from the simulation in units of 10^{21} m^{-3} s^{-1} (top row) and measured plasma emission at 250 nm in a.u. (bottom row) in a CF_4 discharge at different pressures (13.56 MHz, 200 V).

function of pressure due to enhanced electron attachment. Consequently, the drift and ambipolar fields both increase as a function of pressure.

We note that the ability of the simulation to reproduce the measured spatiotemporal emission, strongly depends on the ion-ion recombination rate. In the literature, different values ranging from 1×10^{-13} m^3 s^{-1} [21] to 5.5×10^{-13} m^3 s^{-1} [12] are found. Using a lower value of 1×10^{-13} m^3 s^{-1} instead of 5.5×10^{-13} m^3 s^{-1}, we observe spatial striations of the ionization rate, which are not observed experimentally. This might indicate that 5.5×10^{-13} m^3 s^{-1} is the correct rate.

In conclusion, we investigated a novel operation mode of electronegative CF_4 CCRF discharges characterized by ionization in the bulk and at the sheath edges at distinct times within the rf period. An analytical model clarified the physical origin of this Drift-Ambipolar (DA) mode to be (i) a strong drift electric field in the discharge center due to the low dc conductivity caused by the low electron density and (ii) an ambipolar field at the sheath edges due to local maxima of the electron density in the electropositive edge region of the discharge. By increasing the voltage at fixed pressure a transition from the DA- into the α mode is induced, while increasing the pressure at fixed voltage induced a transition from the α- into the DA mode. These transitions were observed both in simulations and experiments. Our model predicts a high drift field in the bulk to be also caused by a high electron-neutral collision frequency, i.e., at high pressures, such as observed in APPJs. Finally, we note, that the DA mode has important effects on the operation of electrically asymmetric dual-frequency CCRF discharges in CF_4, where it affects the electrical generation of a dc self-bias via the electrical asymmetry effect [22] and limits the quality of separate control of the average ion energy and flux at the electrodes [15].

Funding: Hungarian Fund for Scientific Research (OTKA K77653), RUB Research Department Plasma, Alexander von Humboldt Foundation, DFG Collaborative Research Centre TRR24, project B5. We thank U. Czarnetzki for helpful discussions.

[1] G. Gozadinos, M. M. Turner, and D. Vender, Phys. Rev. Lett. **87**, 135004 (2001); M. M. Turner, J. Phys. D **42**, 194008 (2009); I. D. Kaganovich, Phys. Rev. Lett. **89**, 265006 (2002); T. Mussenbrock *et al.*, Phys. Rev. Lett. **101**, 085004 (2008); V. A. Godyak, R. B. Piejak, and B. M. Alexandrovich, Phys. Rev. Lett. **68**, 40 (1992); M. M. Patterson *et al.*, Plasma Sources Sci. Technol. **16**, 257 (2007).

[2] J. Schulze *et al.*, J. Phys. D **41**, 195212 (2008); J. Schulze *et al.*, J. Phys. D **41**, 042003 (2008).

[3] K. Dittmann *et al.*, J. Phys. D **40**, 6593 (2007); K. Dittmann *et al.*, Contrib. Plasma Phys. **50**, 942 (2010).

[4] J. Schulze *et al.*, J. Phys. D **41**, 105214 (2008).

[5] M. A. Lieberman and A. J. Lichtenberg, *Principles of Plasma Discharges and Materials Processing* (Wiley Interscience, Hoboken, NJ, 2005), 2nd. ed.

[6] K. H. Becker *et al.*, J. Phys. D **39**, R55 (2006); J. J. Shi and M. G. Kong, Phys. Rev. Lett. **96**, 105009 (2006); F. Iza, J. K. Lee, and M. G. Kong, Phys. Rev. Lett. **99**, 075004 (2007).

[7] J. Benedikt *et al.*, Eur. Phys. J. D **60**, 539 (2010).

[8] J. Waskoenig *et al.*, Plasma Sources Sci. Technol. **19**, 045018 (2010).

[9] Ph. Belenguer and J. P. Boeuf, Phys. Rev. A **41**, 4447 (1990).

[10] J. Schulze *et al.*, Plasma Sources Sci. Technol. **19**, 045028 (2010); J. Waskönig and T. Gans, Bull. Am. Phys. Soc. BAPS.2009.GEC.FT1.4 (2009).

[11] M. J. Kushner, IEEE Trans. Plasma Sci. **14**, 188 (1986).

[12] O. V. Proshina *et al.*, Plasma Sources Sci. Technol. **19**, 065013 (2010).
[13] M. Yan *et al.*, Plasma Sources Sci. Technol. **9**, 583 (2000).
[14] I. V. Schweigert, Phys. Rev. Lett. **92**, 155001 (2004).
[15] J. Schulze *et al.*, Plasma Sources Sci. Technol. **20**, 045008 (2011).
[16] V. Georgieva *et al.*, J. Appl. Phys. **93**, 2369 (2003).
[17] J. Schulze *et al.*, J. Phys. D **43**, 124016 (2010); T. Gans *et al.*, Phys. Rev. A **67**, 012707 (2003).
[18] U. Müller *et al.*, Z. Phys. D **24**, 131 (1992).
[19] M. Kurihara *et al.*, J. Phys. D **33**, 2146 (2000); V. Georgieva, A. Bogaerts, and R. Gijbels, Phys. Rev. E **69**, 026406 (2004).
[20] A. V. Phelps (unpublished), http://jila.colorado.edu/~avp/collision_data/.
[21] S. Rauf and M. J. Kushner, J. Appl. Phys. **82**, 2805 (1997).
[22] J. Schulze *et al.*, J. Phys. D **42**, 092005 (2009); U. Czarnetzki *et al.*, Plasma Sources Sci. Technol. **20**, 024010 (2011).